

## Numerical simulation of 7075 Aluminium alloy under high strain rates with different striker bar velocities of split Hopkinson pressure bar

Yasir Majeed Bhat<sup>1</sup>, Sachin saini<sup>2</sup>, Ajay Rana<sup>3</sup>

<sup>1</sup> Mechanical Engineering Department, RIMT University, India

<sup>2</sup> Mechanical Engineering Department, RIMT University, India

<sup>3</sup> Mechanical Engineering Department, RIMT University, India

### ABSTRACT

A research was carried out to observe the dynamic properties of 7075 Aluminium Alloy by employing SHPB simulation with different velocities of the impacting bar. Cylindrical and square specimens of standard diameter were compressed at high rates of strain. It is essential to comprehend how materials behave in dynamic circumstances like bullet penetration, vehicle crashworthiness, blasts, and explosions. Although experimental techniques like split Hopkinson pressure bar and Taylor impact tests can be used to characterize materials at high strain rates, they can be expensive and challenging. Nonetheless, it is feasible to describe materials when subjected to dynamic conditions by utilizing the finite element software of split Hopkinson pressure bar test during loadings with high strain rates. To examine the effect of velocity at high strain rates, numerical simulations of 7075 aluminum alloy were carried out using Abaqus/Explicit 6.14 under different striker bar velocities, varying from 20m/s to 100m/s. The study also analyzed the effects of sample aspect ratio underneath dynamic conditions. The results showed that the wave properties and flow curve of 7075 aluminum alloy depend on striker speeds. A constitutive equation was utilized to explain the dynamic impact deformation behavior of 7075 aluminum alloy, taking into consideration the influence of temperature, strain hardening, strain rate sensitivity, and thermal softening of the material, which was found to be successful.

**Keywords:** split Hopkinson pressure bar, numerical simulation, 7075 Al alloy, finite element analysis

Date of Submission: 09-05-2023

Date of acceptance: 20-05-2023

### I. Introduction

The critical engineering alloy AA7075 has become widely used in aerospace and armor structures due to its high ratio of strength to density. Extensive research has been conducted on its plastic flow at various temperatures and low strain rates. Nevertheless, there has been limited work on understanding the impact of high strain rates on this material during dynamic deformation. To gain a comprehensive understanding of the deformability of AA7075, it's crucial to characterize its dynamic performance over a wide range of strain rates, including those resulting from dynamic impact loading [1].

The importance of understanding the behavior of aluminum alloy AA7075 under dynamic loading conditions remains significant due to its widespread use in space manufacturing, mechanical resources, and astronomical machinery [2]. In 1872, Hopkinson utilized the Hopkinson bar experimental method to investigate the impact characteristics of iron wires. Later on, several researchers made

modifications to the Hopkinson bar to obtain accurate pressure vs. time graphs, error-free wave scattering, and strains. To observe the varying heights at which wave's peak and trough, new methods such as the pulse refining system and the elongated striker's technique have been developed. Numerical research into the effects of pulse shaping techniques is conducted using the SHPB instrument [3].

Because of its widespread application in space manufacturing, mechanical resources, and astronomical machinery, research into the behaviour of aluminium alloy AA7075 under dynamic loading situations has constantly remained significant [4]. In 1872, Hopkinson utilised the Hopkinson bar experimental method to investigate the impact features of iron wires. Several researchers later made adjustments to the Hopkinson bar to obtain accurate pressure vs time graphs, error-free wave scattering, and strains. In order to observe the varying heights at which waves peak and trough, several new methods, including the pulse refining

system and the elongated strikers technique, have been developed [5]. The SHPB instrument is used for numerical research into the effects of pulse shaping techniques [6]. Ductile alloys' behaviour in SHPB was studied by Chen et al. Lee and Lin [7] in their study, Chen et al., Lee, and Lin used the SHPB system to investigate the dynamic behavior of two different ductile alloys, namely pure copper and an aluminum alloy (Al6061-T6), at strain rates ranging from 1000 to 5000  $s^{-1}$ . The researchers aimed to cognize how the mechanical properties of these materials change with increasing strain rates. The outcomes of the study showed that the mechanical performance of the two ductile alloys differed significantly at high strain rates. The pure copper material exhibited higher strain rate sensitivity than the aluminum alloy, meaning that its mechanical properties were more sensitive to changes in strain rate. Additionally, the scholars witnessed that the ductility of both materials decreased with growing strain rate. Overall, the study by Chen et al., Lee, and Lin provides valuable insights into the performance of ductile alloys underneath high strain rate conditions, which can be useful in the development of materials for high-speed impact and deformation applications. Kajberg and Sundin [8] use a SHPB-equipped heating cradle to monitor the response of steels at elevated temperatures. Using finite element analysis, the belongings of radial apathy and abrasion on pure aluminium 1100 were investigated while subjected to a great strain level. Yang et al. [9] examined the characteristics of Al/PTFE under high strain rate. The simulation shows that with extreme shock pressure, the Teflon matrix melts. Atomic diffusion was sped up by PTFE melts and breakdown. As a result, rather than detonating, the Al/PTFE composites' reactions are more akin to combustion. Wen et al. [10] noticed the compressive response of porcine muscle using an improved SHPB. The outcomes show that the flow curves in the two loading axis are delicate to strain loading. The stress along the direction of fiber is stiffer than the stress to the fiber's normal direction. The strength of the muscle was analyzed at varying strain degrees, and a constitutive model that is strain proportion dependent was developed and then formfitting to the investigational records. The outcomes validate the constitutive simulation's capability to illustrate the dynamic properties of the muscle. By conducting simulation of SHPB for concrete samples, Li et al. [11] compared the flow behaviour of the two shapes of samples. Numerical simulation results were analysed in depth, and it was found that, for a given strain rate, the cylindrical specimen exhibited greater lateral inertial confinement than the cubic specimen. Due to the decreased crosswise captivity and appearance of

tensile stress in the cubic specimen, the corners were damaged more severely than in the cylindrical specimen. Han et al. [12] observed the cracking development and final catastrophe designs of a sandwiched cement mortar using SHPB equipped with a camera under high strain rates. When composite specimens deform, the layer of cement mortar might act as a cushion. The digital images demonstrate that, independent of the interlayer properties, tensile cracks often start at the boundary, spread lengthwise the loading track, and ultimately lead to tensile catastrophe. Laizhou granite was subjected to a high strain loading test by Wang et al. [13] utilizing the SHPB method and a high-speed 3D arithmetical image association approach. Cui et al. Cui et al. established a concrete model to analyze the outcome of strain loading on concrete under restraining forces, taking into account the presence of haphazardly dispersed masses. The study found that the impact of strain stacking on concrete is less pronounced in stress states that are not uniaxial, and this effect decreases as the confining pressure increases. In other words, the study suggests that the consequence of strain loading on concrete depends on the stress state of the material, with a smaller effect observed when the material is subject to more complex stress states. Additionally, the study found that as the restraining pressure on the concrete increases, the effect of strain loading on the material decreases. Overall, the study provides insight into the behavior of concrete under different types of loading and can help inform the design and construction of concrete structures. To learn how varying amounts of grease affected the behavior of the concrete in SHPB, Kim et al. [14] led experiments and finite elements simulations of SHPB. The experimental and numerical results showed that after an emollient concentration greater than or equivalent to 12 milligram per centimeter square was realistic to the sample in the concrete SHPB test, the frictional effect was eliminated. Pajak et al. [15] conducted SHPB compression testing on three different types of Self-compacting concrete (SCC) at strain fluctuating beginning 68 to 236  $s^{-1}$ . A systematic approach is provided for conducting SHPB testing of SCC in a reliable and time-saving manner. To characterize the three parts of the 3D mesoscale that were built—mortar, the Interface transition zone, and arbitrarily created collective spheres—the authors employed the Johnson-Holmquist material model [16]. Outcomes from SHPB testing revealed that the material's properties and the indolence impact are the reasons of the DIF. The importance of crosswise inertial captivity, which is found to be strength-dependent, decreases at strain loadings outside 200 $s^{-1}$ . You et al. [17] used an altered SHPB system to examine the

responses and breakage processes of 3D restricted fractured rocks exposed to quasi and vigorous strain rate. The outcomes exhibited that underneath greater axial pressures, the dynamic pressure is extra reactive to strain loading, and that together the dynamic and whole strengths have noteworthy constructive lined connections with strain loading. Pająk and Janiszewski [18] studied the influence of reinforcement of steel fibers in the cement mortar mixture aggregates under high rate of loadings. The study showed that the tested mixtures all had a significant strain rate influence. It was furthermore discovered that the coarse aggregate has a negligible effect on the sensitivity of mortar to changes in strain rate [19]. Both concrete and mortar benefited greatly from the addition of fibers, as their strain rate sensitivity was greatly diminished [20]. Ma et al. [21] observed the dynamic and constitutive behaviour of alumina under dynamic strain range and found that on strain degrees beyond an acute assessment, the catastrophe strength of alumina was initiate, to remain highly reliant on the strain loading. The dynamic stress-strain curves showed inelastic deformation, indicating that modulus degradation does occur [22]. Research on SHPB loads has shown that reducing the impact velocity can reduce the impact of interfacial friction, allowing uniaxial loading to be maintained. Finally, since alumina is relatively unaffected by inter-facial resistance inside range of the attainable strain loading, it is recommended that a characteristic proportion of 1.0 be used for the sample [23]. To examine the power of sample shape and magnitude on concrete compressive strength at varying loading rates, Li et al. [24] produced and tested concrete examples of varying dimensions, both cubic and cylindrical, under varying loads. There was a call for empirical relationships to be developed to help make sense of the discrepancy between the varying loads of concrete samples of altered forms and dimensions. Swamy et al. [25] studied the wear behavior of a hybrid metal matrix composite coating made of Al7075 with the reinforcement of Gr micro particles and nano TiO<sub>2</sub> particles. Husain et al. [26] examined the wear performance of Al-7075 alloys that were reinforced with Mica and Kaolinite. Wekezer et al. [27] developed a comprehensive testing approach for truck tires that involved multiple stages, including quasi-static, dynamic, and strongly dynamic tests. Krishana et al. [28] conducted research on the synthesis of Al7075 and

Al<sub>2</sub>O<sub>3</sub> powders using high-energy ball milling and found that the grain size was refined, resulting in better density, Vickers microhardness, and corrosion resistance. Yang et al. [29] conducted a study on the behavior of Al/PTFE under high strain rate conditions, finding that under extreme shock pressure, the Teflon matrix melted, which led to reactions that were more similar to combustion than detonation. Finally, Han et al. [30] studied the cracking behavior and failure modes of a sandwiched cement mortar under high strain rates using an SHPB and camera, discovering that tensile cracks generally initiated at the boundary, propagated along the loading track, and ultimately resulted in tensile failure, irrespective of the interlayer properties. Ma et al. [31] examine the behavior of alumina under dynamic strain ranges and find that the catastrophic strength of alumina is highly dependent on the strain loading beyond a critical threshold. Li et al. [32] investigate the effect of sample shape and size on concrete compressive strength under varying loading rates and propose empirical relationships to address the differences in compressive strength of concrete samples with varying shapes and dimensions. Zhang et al. [33] study the creep behavior of 7075 under different conditions and find that the intensity of the Cu texture increases with elevated temperature and equivalent stress [34]. The paper presents a numerical simulation of AA7075 using SHPB with different striker bar configurations to better understand the impact of these modifications. The impact of the sample's aspect ratio is also being examined to understand how the wave fields adapt to alterations in the sample dimensions. [35].

## II. Methodology

In this study, the aim is to explore the dynamic behavior of AA7075 aluminum alloy at high strain rates by modifying the velocity of the striker bar, while keeping the specimen diameter constant. To investigate the effects of striker bar velocity on the flow curve of AA7075, Abaqus software is utilized. Additionally, the research examines the effects of strain rate sensitivity and aspect ratio by conducting simulations of AA7075 at various striker velocities (ranging from 20 to 100 m/s) and with different specimen shapes, such as circular and square.

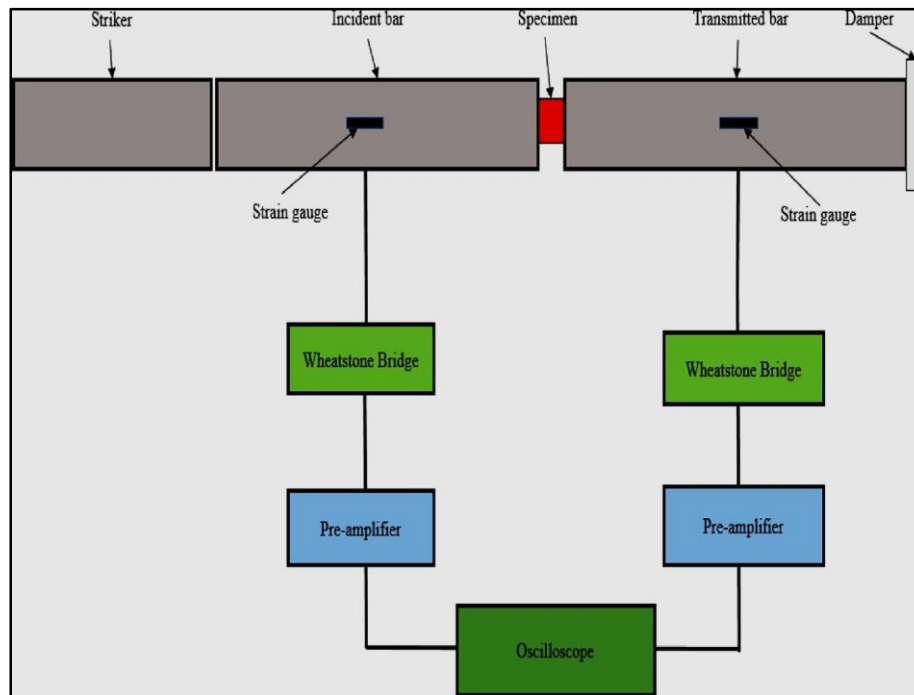


Fig. 1 showing mesh model of SHPB in ABAQUS

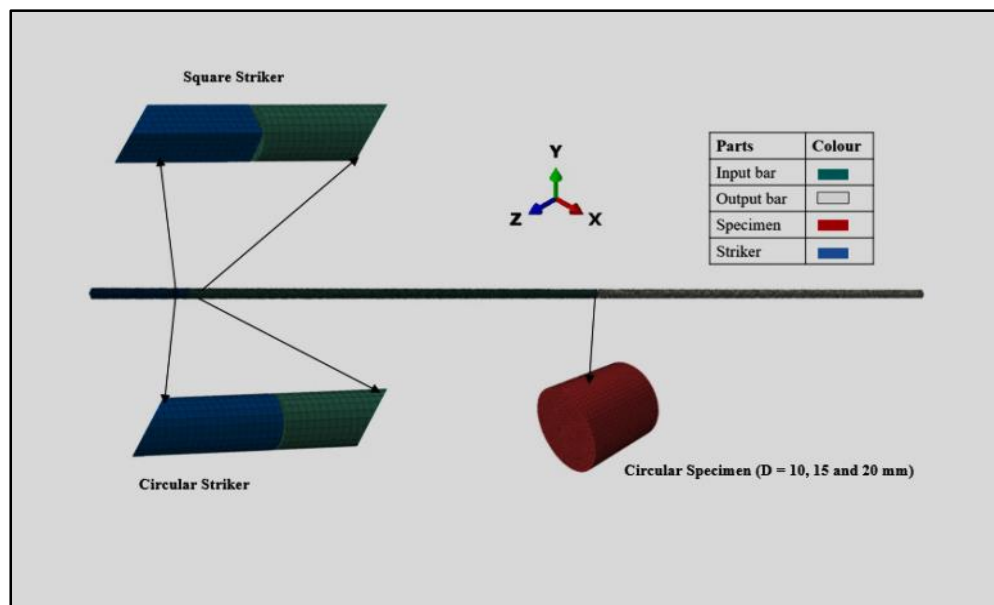


Fig. 2 showing the schematic view of SHPB

### III. Split Hopkinson pressure bar

The SHPB (Split Hopkinson Pressure Bar) technique is a versatile approach utilized to determine the mechanical characteristics of materials under high strain rates. By means of the SHPB experimental configuration, it is possible to carry out tests on samples subjected to tension, compression, and shear forces, in order to obtain the

corresponding stress-strain curves. The SHPB equipment consists of three main elements: an incident bar, a transmitter bar, and a striker. The sample is placed between the incident and transmitter bars. Upon releasing a high-velocity stream from the compressor, the striker bar acquires energy, resulting in the generation of an incident stress wave that propagates along the incident bar

until it collides with the sample. A portion of the incident stress wave is reflected back from the interface of the bar and sample as a reflected wave, while the remaining part transmits through the sample due to the wave impedance mismatch. The transmitted wave from the sample travels along the transmitter bar until it reaches the end of the bar. Strain sensors placed equally on each bar gauge the strains generated by the incident wave, reflected wave, and transmitted wave as a function of time, and the data is saved in an appropriate device such as an amplifier and software, which generates the final stress-strain curves. As the wave travels through the sample, it undergoes plastic deformation at a high rate of strain, necessitating multiple reflections within the sample to achieve equilibrium stress. To evaluate the axial components of stress ( $\sigma$ ), strain ( $\epsilon$ ), and strain rate ( $\dot{\epsilon}$ ) in the sample, three time-dependent elastic stress waves (incident, reflected, and transmitted) are measured using strain sensors attached to pressure bars and recorded using a digital oscilloscope. In the event of dynamic equilibrium where stress is uniform throughout the sample, the equations for strain rate, strain, and stress can be expressed as follows:

$$\dot{\epsilon}_s(t) = -\frac{2C}{L_S} \epsilon_R(t) \quad (1)$$

$$\epsilon_s(t) = -\frac{2C}{L_S} \int \epsilon_R(t) dt \quad (2)$$

$$\sigma(t) = -\frac{AbEb}{As} \epsilon_T(t) \quad (3)$$

In these equations, C represents the elastic wave velocity, LS is the initial length of the specimen, AB and AS denote the cross-sectional areas of the bars and the specimen, respectively, and EB is the Young's modulus of the bar material. These equations are commonly referred to as the one-dimensional wave analysis of SHPB.

#### IV. Finite Element Analysis

The FE analysis program, specifically Abaqus/Explicit 6.14, is utilized for simulating finite elements. The simulation involves creating a 3D model of the SHPB arrangement in ABAQUS to obtain the desired results. As depicted in Figure 1, each component of the Split Hopkinson Pressure Bar is created separately in ABAQUS/Explicit and then assembled. The dimensions of both the SHPB and specimens are outlined in Table 1. The bar material selected has a density of 7800 kg/m<sup>3</sup>, elastic modulus of 200 GPa, and Poisson's ratio of 0.3.

Factors		Sizes (mm)
Striker bar	circular	L = 200, D = 20
Input bar		L = 1000, D = 20
Output bar		L = 1000, D = 20
Specimen	Circular Square	L = 10, D = 10 L = 10, S = 7.07

Table 1 showing the Geometric properties of SHPB

For the AA7075 sample, the Johnson-Cook Material model is utilized. This model is commonly used to characterize specimens under dynamic loadings and is frequently applied in SHPB simulations for modeling specimens described by equation 4.

$$\sigma = [A + B\epsilon^n][1 + C \ln \dot{\epsilon}^*][1 - (T^*)^m] \quad 4$$

The Johnson-Cook Material model consists of three components. The first component addresses strain hardening, the second component incorporates strain rate sensitivity, and the third component takes into account the temperature dependence of the material. This model is used to demonstrate the response of specimens under dynamic loadings and in SHPB simulations to model the material's constitutive behavior. The constitutive model constants for AA7075 are presented in Table 2. Furthermore, AA7075 has a density of 2700 kg/m<sup>3</sup>, an elastic modulus of 70 GPa, and a Poisson's ratio of 0.3.

A	B	n	C	m
530 Mpa	480 Mpa	.50	.001	1

Table 2 showing a constitutive model of AA7075 constants

The present study utilized C3D8R elements for meshing the components, with mesh dimensions of 0.28mm and 0.25mm. As per the Abaqus theory manual, C3D8R elements are eight-node brick elements that

are three-dimensional and solid. These elements have an hourglass controller and limited integration. Table 3 provides a summary of the total nodes and elements used in the simulations, along with their respective criteria.

Factors		Total number of elements	Total number of nodes
Striker Velocity	20 m/s	49819	60600
	30 m/s	49819	60600
	40 m/s	49819	60600
	50 m/s	49819	60600
	60 m/s	49819	60600
	80 m/s	49819	60600
	100 m/s	49819	60600
specimen Shape	Circular	49819	60600
	Square	44239	54657

**Table 3 showing Sum of simulated elements and nodes**

The 3D models are meshed and the boundary conditions for the boundaries between the bar to bar and bar to specimen are depicted in Figure 1 using a general contact algorithm. To achieve great strain rates, the striker is attached to the input end with velocities ranging from 20 to 100 m/s. The extreme end of the output bar is retained stationary to measure all forces transmitted through it at the termination end. In order to observe the influence of the specimen's aspect ratio, the diameter of the sample is changed from circular to square while maintaining a constant length of 10 mm.

### V. Validation of FE approach

The validity of the simulation methodology employed in this investigation is demonstrated by relating its outcomes with those stated by Afdal et al. for Al 6063 under dynamic conditions. To ensure the accuracy of the simulation, it was carried out using the same environmental parameters as described in Afdal et al.'s study. Figure 3 presents the results obtained using the current simulation approach for the 6063 Al alloy, which are highly consistent with Afdal et al.'s findings, despite the use of a different approach. This agreement confirms the effectiveness of the numerical method presented in this paper.

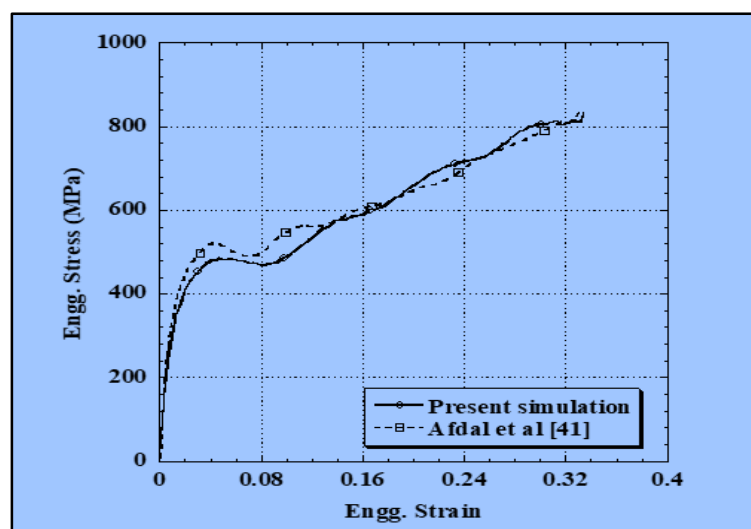


**Figure 3 shows results from the current FE simulation are compared to those obtained by Afdal et al. For Al 6063**

## VI. Results and discussion

The aim of this research is to examine how the stress-strain behavior and wave propagation of AA7075 are affected by variations in striker velocity and specimen diameter through numerical simulation. To accomplish this, we adjusted the velocity of the striker bar within a range of 20 to 1000 m/s to observe its impact on the SHPB components. Moreover, we altered the geometry of the specimen from circular to square to explore the effect of specimen shape on the flow curve and wave dispersion of AA7075 subjected to high strain rates.

Figure 4a shows the wave propagation through the striker bar at different speeds. As the striker bar speed increases, the waves propagate faster and the time interval among the incident and reflected waves reduces. Figure 4b shows the flow curves for AA7075 at different striker velocities. It can be observed that the velocity has a substantial influence on the shape of the flow curves. The ultimate stress is found to be highest at 20 m/s and lowest at 50 m/s for the considered striker velocities. This specifies that the material response is sensitive to the strain rate, which is affected by the striker velocity.

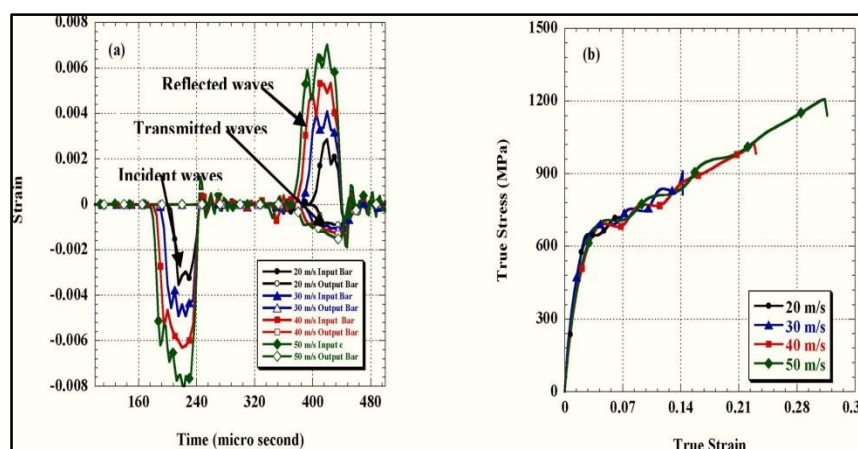


Fig.4 Shows Impact of striker bar velocity on (a) propagation of waves through the input and output bars (b) AA7075's true stress-strain curves.

Figure 5 displays the wave propagation and flow curves of AA7075 at striker velocities oscillating from 60 to 100 m/s. As observed in Figure 5a, the wave propagation is directly proportional to the striker velocity, with 100 m/s generating the highest wave propagation and 60 m/s

generating the lowest. The flow curves in Figure 5b demonstrate that the ultimate stress of AA7075 is highest at 100 m/s and lowest at 60 m/s for the given striker velocities. Hence, at high strain rates, the striker velocity not only affects the wave propagation but also the flow behavior of AA7075.

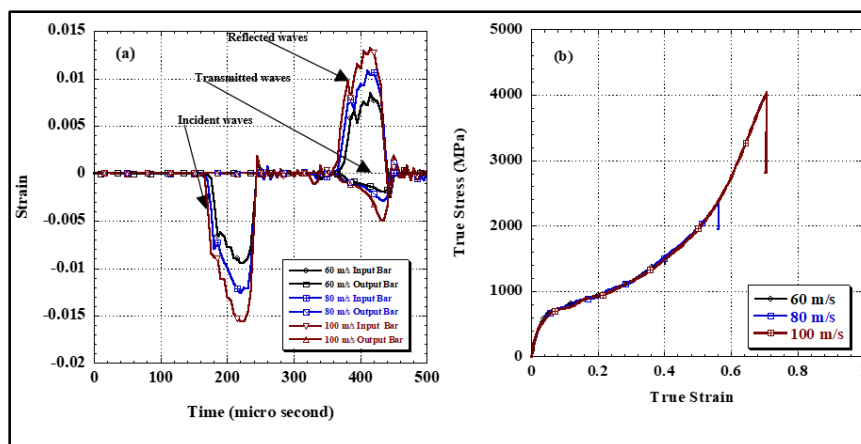


Fig. 5 shows the waves and real flow curves at different speeds of striker bar

Figure 6 presents the impact of specimen shape, with a fixed length of 10mm, on the waves and flow curve of AA7075 at an impact velocity of 60m/s using a circular striker. The square-shaped specimen's cross-sectional area is chosen as 7.07mm, which is the maximum possible area inscribed within a circle with a diameter of 10mm. The incident wave remains unaffected by the change

in specimen shape, as shown in Figure 6a. However, the reflected wave and the incident wave are affected by the change from a circular to a square shape. Figure 6b demonstrates the influence of the specimen form on the real flow curves, with the ultimate compressive strength (UCS) and percentage elongation both highest for the circular specimen and lowest for the square specimen.

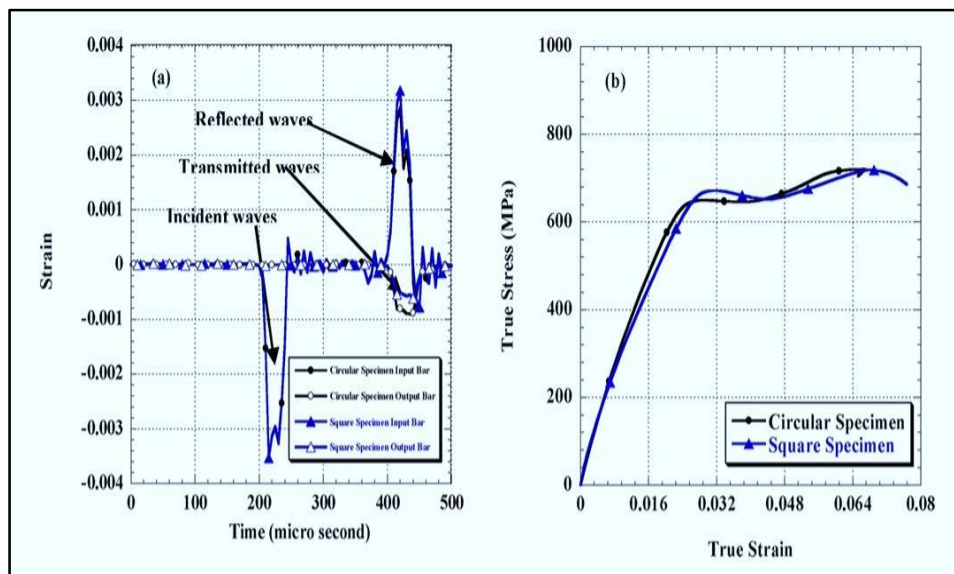


Fig 6 shows the impact of specimen shape on strain rate curves and real flow curves

Factors		True stress strain curve		% elongation
		Yield stress (Mpa)	Ultimate compressive stress (Mpa)	
Striker velocity	20 m/s	275 ± 1	715 ± 1	7.25 ± 0.1
	30 m/s	340 ± 1	915 ± 1	15.21 ± 0.1
	40 m/s	355 ± 1	1025 ± 1	22.07 ± 0.2
	50 m/s	385 ± 1	1205 ± 1	30.62 ± 0.2
	60 m/s	366 ± 1	1501 ± 1	40.21 ± 0.2
	80 m/s	351 ± 1	2357 ± 1	56.15 ± .01
	100 m/s	331 ± 1	4039 ± 1	70.80 ± 0.1
Specimen Shape	Circular	366 ± 1	1501 ± 1	40.21 ± 0.1
	Square	464 ± 1	1340 ± 1	30.84 ± 0.2

Table 4 shows the outcomes of various compression tests

Table 4 displays the actual values for yield strength, ultimate compressive strength, and percent elongation for each simulation run. The results indicate that, for a circular specimen struck by a round striker, increasing the velocity tips to growth in ultimate compressive strength. However, as the striker's speed increases from 20 to 100 m/s, the yield stress falls. The ductility of AA 7075 is highest at a rate of 100 m/s and decreases as the loading rate rises from 20 to 100 m/s. The study's results suggest that the ultimate compressive strength of 7075 is positively influenced by strain

rate at great loading rates. The findings also indicate that changing the sample shape from circular to square leads to an increase in yield strength but a decrease in compressive strength and ductility.

## VII. CONCLUSIONS

In this work, the dynamic properties of AA7075 have been examined through simulations of different striker and specimen geometries. The influence of strain rate has been examined by varying the velocity of the striker bar from 20 to 100 m/s. Furthermore, the behavior of strain waves

propagating through the material has been analyzed under these conditions, resulting in the following findings:

- 1) As the velocity is amplified from 20 to 100 m/s, the peak values of the strain waves are found to increase and decrease, respectively, with the longest and shortest durations being recorded.
- 2) The results of the study display that the ultimate compressive strength (UCS) and ductility of AA7075 are positively influenced by strain rate, while the yield strength is negatively affected by it.
- 3) The incident wave is found to be unaffected by the change in specimen shape.
- 4) The outcomes of the work reveal that the shape of the specimen has a substantial impact on the ductility, yield strength, and ultimate compressive strength of AA7075.
- 5) The study reveals that the ductility of 7075 Aluminium alloy rises as the strain rate rises.

#### ACKNOWLEDGEMENT

The writers are being thankful to RIMT UNIVERSITY for providing us platform for this research work.

#### REFERENCES

- [1] Nishida, M., Hayashi, K., Nakagawa, J., Ito Y.: Influence of temperature on crater and ejecta size following hypervelocity impact of aluminum alloy spheres on thick aluminum alloy targets. *International Journal of Impact Engineering*, 42: 37–47 (2012).
- [2] Liang, X.P., Li, H.Z., Huang, L., Hong, T., Ma, B., Liu, Y.: Microstructural evolution of 2519-T87 aluminum alloy obliquely impacted by projectile with velocity of 816 m/s. *Transactions of Nonferrous Metals Society of China*, 22: 1270–1279 (2012).
- [3] Hopkinson, J.: On the rupture of iron wire by a blow. *Proc. Manchester Literary Philosophical Society*, 11: 40-45.
- [4] Hopkinson, B. A method of measuring the pressure produced in the detonation of high explosives or by the impact of bullets. *Philosophical Transactions of the Royal Society of London Series A: Mathematical, Physical and Engineering Sciences*, 213 (497-508): 437-56 (1914).
- [5] Bancroft, D.: The velocity of longitudinal Waves in cylindrical Bars. *physical Review*, 59: 588-593 (1941).
- [6] Davies, R.M.: A critical study of the Hopkinson pressure bar. *phil. Trans. R. Soc.*, A240: 375-457 (1948).
- [7] Chen, W., Luo, H.: Dynamic compressive responses of intact and damaged ceramics from a single split Hopkinson pressure bar experiment. *Exp. Mech.*, 44: 295–299 (2004).
- [8] Lu, Y., Li, Q.: Appraisal of Pulse-Shaping Technique in Split Hopkinson Pressure Bar Tests for Brittle Materials. *Int. J. Prot. Struct.*, 1, 363–390 (2010).
- [9] Cloete, T., Van Der Westhuizen, A., Kok, S., Nurick, G.N.: A tapered striker pulse shaping technique for uniform strain rate dynamic compression of bovine bone. In *DYMAT—International Conference on the Mechanical and Physical Behaviour of Materials under Dynamic Loading*, Brussels, Belgium, 7–11 September (2009).
- [10] Song, B., Casem, D., Kimberley, J., Eds.: *Springer Science Business Media: Heidelberg, Germany*, 1: 901–907 (2009).
- [11] Bekker, A., Cloete, T., Chinsamy-Turan, A., Nurick, G., Kok, S.: Constant strain rate compression of bovine cortical bone on the Split-Hopkinson Pressure Bar. *Mater. Sci. Eng. C*, 46: 443–449 (2015).
- [12] Baranowski, P., Małachowski, J., Gieleta, R., Damaziak, K., Mazurkiewicz, Ł., Kolodziejczyk, D.: Numerical study for determination of pulse shaping design variables in SHPB apparatus. *Bull. Pol. Acad. Sci. Tech. Sci.*, 61: 459–466 (2013).
- [13] Chen, W., Song, B., Frew, D.J., Forrestal, M.J.: Dynamic small strain measurements of a metal specimen with a split Hopkinson pressure bar. *Exp. Mech.*, 43: 20–23 (2003).
- [14] Lee, W.S., Lin, C.F.: Impact properties and microstructure evolution of 304L stainless steel. *Mater. Sci. Eng. A*, 308: 124–135 (2001).
- [15] Kajberg, J., Sundin, K.G.: Material characterisation using high-temperature Split Hopkinson pressure bar. *J. Mater. Process. Technol.*, 213, 522–531 (2013).
- [16] Zencker, U., Clos, R.: Limiting conditions for compression testing of flat specimens in the split Hopkinson pressure bar. *Exp. Mech.* 39: 343–348 (1999).
- [17] Yang XL, He Yong, He Yuan, Wang CT and Zhou J. Investigation of the shock compression behaviors of Al/PTFE composites with experimental and a 3D mesoscale-model, *Defence Technology* 2022; 18(1), 62-71.
- [18] Wen Y, Xu L, Chen A, Dong F and Qin B. Dynamic compressive response of porcine muscle measured using a split Hopkinson bar system with a pair of PVDF force transducers, *Defence Technology* 2022.
- [19] Li M, Hao H, Cui J and Hao Y. Numerical investigation of the failure mechanism of cubic concrete specimens in SHPB tests. *Defence Technology* 2022; 18(1), 1-11.

- [20] Han Z, LiD and Li X. Dynamic mechanical properties and wave propagation of composite rock-mortar specimens based on SHPB tests. *International Journal of Mining Science and Technology* 2022; 32(4), 793-806.
- [21] WangJ, Ma L, Zhao F,Lv B, Gong W,He Mand LiuP. Dynamic strain field for granite specimen under SHPB impact tests based on stress wave propagation. *Underground Space* 2022; 7(5), 767-785.
- [22] Cui J, Hao J and Shi Y. Numerical study of the influences of pressure confinement on high-speed impact tests of dynamic material properties of concrete. *Construction and Building Materials* 2018; 171, 839-849.
- [23] Kim KM, Lee S and Cho JY. Influence of friction on the dynamic increase factor of concrete compressive strength in a split Hopkinson pressure bar test. *Cement and Concrete Composites*, Volume 129, May 2022, 104517.
- [24] Pajak M, Baranowski P, Janiszewski J, Kucwicz M, Mazurkiewicz L andPiekarczyk B. Experimental testing and 3D meso-scale numerical simulations of SCC subjected to high compression strain rates. *Construction and Building Materials*, Volume 302, 4 October 2021, 124379.
- [25] You W, Dai F and Liu Y. Experimental and numerical investigation on the mechanical responses and cracking mechanism of 3D confined single-flawed rocks under dynamic loading. *Journal of Rock Mechanics and Geotechnical Engineering*, Volume 14, Issue 2, April 2022, Pages 477-493.
- [26] Małgorzata Pajak and Jacek Janiszewski, Influence of aggregate and recycled steel fibres on the strain rate sensitivity of mortar and concrete, *Construction and Building Materials* Volume 363, 11 January 2023, 129855.
- [27] Yuanyuan Ma, Zhiyong Wang and Youquan Qin. Impact of characteristic length and loading rate upon dynamic constitutive behavior and fracture process in alumina ceramics, *Ceramics International*, Volume 49, Issue 3, 1 February 2023, Pages 4775-4784.
- [28] Li M, Hao H, Shi Y and Hao Y. Specimen shape and size effects on the concrete compressive strength under static and dynamic tests. *Construction and Building Materials*, Volume 161, 10 February 2018, Pages 84-93.
- [29] Markovsky PE, Janiszewski J, Savvakin DG, Stasiuk OO, Cieplak K, Baranowski P and Prikhodk SV. Mechanical behavior of bilayer structures of Ti64 alloy and its composites with TiC or TiB under quasi-static and dynamic compression. *Materials & Design*, Volume 223, November 2022, 111205.
- [30] Markovsky PE, Janiszewski J, Dekhtyar OI, Mecklenburg M and Prikhodko SV. Deformation mechanism and structural changes in the globular Ti-6Al-4V alloy under quasi-static and dynamic compression. To the question of the controlling phase in the deformation of  $\alpha+\beta$  titanium alloys. *Crystals*, 12 (2022), p. 645, 10.3390/cryst12050645.
- [31] Markovsky PE, Janiszewski J, Stasiuk OO, Bondarchuk VI, Savvakin DG, Cieplak K,Goran KD, Soni P and Prikhodko S.Mechanical behavior of titanium based metal matrix composites reinforced with TiC or TiB particles under quasi-static and high strain-rate compression. *Materials*, 14 (22) (2021), p. 6837, Zhang L. Thermo-mechanical characterization and dynamic failure of a CoCrFeNi high-entropy alloy. *Materials Science and Engineering: A*. Volume 844, 2 June 2022, 143166.